# Arabidopsis V-ATPase activity at the tonoplast is required for efficient nutrient storage but not for sodium accumulation

Melanie Krebs[a], Diana Beyhl[b], Esther Görlich[a], Khaled A. S. Al-Rasheid[c], Irene Marten[b], York-Dieter Stierhof[d], Rainer Hedrich[b], and Karin Schumacher[a,1]

[a]Heidelberg Institute for Plant Sciences, University of Heidelberg, 69120 Heidelberg, Germany; [b]University of Wuerzburg, Biocenter, Institute for Molecular Plant Physiology and Biophysics, D-97082 Wuerzburg, Germany; [c]King Saud University, College of Science, Center of Excellence in Biodiversity Research, Riyadh 11451, Saudi Arabia; and [d]Center for Plant Molecular Biology-Microscopy, Universität Tübingen, 72076 Tübingen, Germany

Edited* by Maarten J. Chrispeels, University of California at San Diego, La Jolla, CA, and approved December 28, 2009 (received for review November 11, 2009)

**The productivity of higher plants as a major source of food and energy is linked to their ability to buffer changes in the concentrations of essential and toxic ions. Transport across the tonoplast is energized by two proton pumps, the vacuolar $H^+$-ATPase (V-ATPase) and the vacuolar $H^+$-pyrophosphatase (V-PPase); however, their functional relation and relative contributions to ion storage and detoxification are unclear. We have identified an Arabidopsis mutant in which energization of vacuolar transport solely relies on the activity of the V-PPase. The *vha-a2 vha-a3* double mutant, which lacks the two tonoplast-localized isoforms of the membrane-integral V-ATPase subunit VHA-a, is viable but shows day-length-dependent growth retardation. Nitrate content is reduced whereas nitrate assimilation is increased in the *vha-a2 vha-a3* mutant, indicating that vacuolar nitrate storage represents a major growth-limiting factor. Zinc is an essential micronutrient that is toxic at excess concentrations and is detoxified via a vacuolar $Zn^{2+}/H^+$-antiport system. Accordingly, the double mutant shows reduced zinc tolerance. In the same way the vacuolar $Na^+/H^+$-antiport system is assumed to be an important component of the system that removes sodium from the cytosol. Unexpectedly, salt tolerance and accumulation are not affected in the *vha-a2 vha-a3* double mutant. In contrast, reduction of V-ATPase activity in the trans-Golgi network/early endosome (TGN/EE) leads to increased salt sensitivity. Taken together, our results show that during gametophyte and embryo development V-PPase activity at the tonoplast is sufficient whereas tonoplast V-ATPase activity is limiting for nutrient storage but not for sodium tolerance during vegetative and reproductive growth.**

proton-pump | pH-homeostasis | vacuole | nitrate | salt tolerance

The productivity of higher plants as a major source of food and renewable energy is linked to their ability to cope with fluctuations in essential as well as toxic ion and metabolite concentrations. In plants the large central vacuoles function as reservoirs for ions and metabolites that allow buffering of changes in nutrients as well as challenges by toxic components that plants, as sessile, photoautotrophic organisms, frequently encounter. Furthermore, vacuoles are essential for plant growth and development. Expansion of plant cells is achieved by osmotically driven water influx into the vacuole that, in combination with the cell wall, generates turgor, the driving force for hydraulic stiffness and plant growth.

All vacuolar functions require massive fluxes of ions and metabolites that are channeled by a battery of vacuolar transport proteins, many of which have been well characterized physiologically, but the nature of several transporters remains to be identified (1). Among those characterized on the molecular level are, e.g., those transporting $NO_3^-$, $Na^+$, and protons. Nitrate, a major plant nutrient, is accumulated and stored in the vacuole from where it can be retrieved according to metabolic demands (2). Uptake into the vacuole is achieved by proton-coupled anion transport (3) that has been shown to be mediated by AtCLCa, a member of the CLC family of anion channels that acts as a $NO_3^-/H^+$ exchanger (4). A similar proton antiport mechanism has long been known to be responsible for vacuolar uptake of sodium (5). Soil salinity poses a major limitation in agriculture and sodium accumulation in the vacuole provides a strategy to avoid toxicity in the cytosol. Overexpression of AtNHX1, a vacuolar $Na^+/H^+$-antiporter in Arabidopsis, resulted in plants exhibiting increased salt tolerance (6); however, on the basis of the respective loss-of-function phenotype (7) it seems likely that other mechanisms contribute to vacuolar sodium accumulation as well.

Transport across the delimiting membrane, the tonoplast, is energized by two proton pumps, the vacuolar $H^+$-ATPase (V-ATPase) and the vacuolar $H^+$-pyrophosphatase (V-PPase) (8). The combined activity of the two pumps creates the proton gradient and the membrane potential that is used to transport compounds against their concentration or electrochemical gradients (9).

V-ATPases are highly conserved, multisubunit proton pumps that consist of two subcomplexes. The peripheral $V_1$ complex, which consists of eight subunits (VHA-A to -H), is responsible for ATP hydrolysis, whereas the membrane-integral $V_0$ complex (VHA-a, -c, -c′, -c′′, -d, and -e) is responsible for proton translocation from the cytosol into the lumen of endomembrane compartments (10). In comparison with the V-ATPase, the V-PPase, a homodimer of a single polypeptide, is a much simpler enzyme that uses energy of the phosphoanhydride bond of pyrophosphate ($PP_i$) to drive proton transport across membranes (9, 11). Both proton pumps are among the most abundant tonoplast proteins (12, 13), indicating that the amount of energy invested into vacuolar transport is substantial. $PP_i$ is a by-product of several biosynthetic processes and it has therefore been argued that the V-PPase is the predominant proton pump in the vacuoles of young, growing cells (14). The V-PPase has also been discussed as a backup system for the V-ATPase under ATP-limiting conditions like anoxia and cold stress (11). Due to their different energy sources it is generally assumed that the combined action of the two enzymes enables plants to maintain transport into the vacuole even under stressful conditions. The

Author contributions: M.K., K.A.S.A.-R., R.H., and K.S. designed research; M.K., D.B., E.G., and Y.-D.S. performed research; M.K., D.B., I.M., R.H., and K.S. analyzed data; and M.K. and K.S. wrote the paper.

The authors declare no conflict of interest.

*This Direct Submission article had a prearranged editor.

[1]To whom correspondence should be addressed. E-mail: karin.schumacher@hip.uni-heidelberg.de.

This article contains supporting information online at www.pnas.org/cgi/content/full/0913035107/DCSupplemental.

PLANT BIOLOGY

functional relation and relative contributions of the two vacuolar proton pumps remain to be determined.

The analysis of mutants lacking one of the two vacuolar proton pumps promises insights into their biological functions in different tissues, developmental stages, or stress situations but the function of V-ATPase and V-PPase is not limited to the tonoplast. So far, mutant analysis has uncovered important functions for both pumps in endocytic and secretory trafficking but has not contributed to a delineation of their vacuolar functions. Null alleles for Arabidopsis V-ATPase genes cause either gametophytic or embryo lethality (15, 16) and even a 2-fold reduction of V-ATPase activity as found in *de-etiolated 3* (*det3*) causes severe growth defects (17) due to reduced V-ATPase activity in the trans-Golgi network/early endosome (TGN/EE) (18). Similarly, a null allele of the ubiquitously expressed V-PPase AVP1 causes a severe phenotype related to a defect in endosomal trafficking of the auxin-efflux carrier PIN1 and consequently polar auxin transport (19).

We have recently shown that the three Arabidopsis isoforms of the membrane-integral subunit VHA-a are differentially localized in the TGN/early endosome (VHA-a1) and in the tonoplast (VHA-a2, VHA-a3). On the basis of this result, we have created a double mutant that specifically lacks V-ATPase at the tonoplast. We show here that although the V-PPase is sufficient for survival under certain conditions, tonoplast V-ATPase activity is required for efficient nitrate storage and metal sequestration. Surprisingly, we found that tonoplast V-ATPase activity is not limiting for sodium accumulation. In contrast, salt sensitivity is increased in plants with reduced V-ATPase in the TGN/EE, pointing to an important role of the endosomal system in sodium uptake and toxicity.

## Results

**A Mutant Lacking VHA-a2 and VHA-a3 Has No Tonoplast V-ATPase Activity.** Arabidopsis has three isoforms of the membrane-integral V-ATPase subunit VHA-a that are differentially localized. Whereas VHA-a1 is found in the TGN/early endosome, VHA-a2 and VHA-a3 are both found at the tonoplast (18, 20). To determine the phenotype of plants that lack V-ATPase at the tonoplast, we combined a previously described T-DNA null allele of *VHA-a3* (18) with a T-DNA line carrying an insertion in *VHA-a2*. The T-DNA line (SALK_142642) carrying an insertion in exon 3 of *VHA-a2* (chromosome 2, position 9,163,254, Fig. S1*A*) was obtained from the SALK collection (21). Homozygous *vha-a2* individuals were identified by PCR. RT-PCR showed that *vha-a2* is a null allele, as the full-length *VHA-a2* transcript was not detectable (Fig. S1*B*). Double mutants identified in the $F_2$ derived from a cross of homozygous *vha-a2* and *vha-a3* individuals showed severely reduced rosette size (Fig. S1*C*). Surprisingly, by RT-PCR a truncated *VHA-a2* transcript was detected in the double mutant (Fig. S1*B*). Sequencing revealed that the exon carrying the T-DNA is spliced out along with its two flanking introns (Fig. S1*A*). Analysis of the kanamycin resistance (KanR) in the single and double mutants indicates that this unusual splicing behavior goes along with silencing of the 35S promotor driving the neomycin phosphotransferase gene (*NPTII*) on SALK_142642 (Fig. S2*A*). This result was further substantiated by combining the *vha-a2* T-DNA allele with an independent T-DNA insertion carrying a silenced *NPTII* gene (Fig. S2*A*) as well as by crossing the activation-tagged *pap1-D* (22) allele into the *vha-a2 vha-a3* background (Fig. S2 *C–E*).

Given the unusual splicing behavior of *vha-a2* that goes along with transinactivation of the 35S promotor driving the *NPTII* gene on the T-DNAs used to create the SALK and other insertion collections (23), combinations of multiple insertion alleles require detailed analysis of the individual transcript levels. To our knowledge similar cases of silencing-induced exon splicing have not been reported. Although exon splicing may be a rare event, it seems prudent to take this phenomenon into account, at least when combinations of multiple insertion alleles result in unexpected phenotypes.

The transcript present in *vha-a2 vha-a3* encodes a protein that lacks 41 aa in the N-terminal cytosolic domain. We examined if this truncated protein could be functional. Immunogold electron microscopy using an antibody against VHA-E (16) failed to detect $V_1$ compexes at the tonoplast of *vha-a2 vha-a3* seedlings (Fig. S3*A*), indicating that the amount of V-ATPase complexes at the tonoplast is at least severely reduced. Furthermore, the patch-clamp technique was applied to determine if the double mutant has residual tonoplast V-ATPase activity. ATP-induced membrane polarizations (Fig. 1*A*) as well as ATP-stimulated proton currents (Fig. S3*B*) were recorded in the whole-vacuole configuration and provided unequivocal evidence that *vha-a2 vha-a3* vacuoles are devoid of V-ATPase activity. This result is consistent with the finding that localization of VHA-a1-GFP is not affected in *vha-a2 vha-a3* mutant cells and that the presence of an additional copy of *VHA-a1* does not restore growth of the double mutant (Fig. S4 *A* and *B*). Furthermore, VHA-a2 and VHA-a3 are both found at the tonoplast of mature central-vacuoles and of small undifferentiated vacuoles (Fig. S4*C*).

**Proton-Pump Activity and Vacuolar pH.** Viability of *vha-a2 vha-a3* plants could be due to increased activity of the V-PPase and the activity of both pumps was thus determined. Total V-ATPase activity in microsomal extracts from etiolated seedlings of WT, *vha-a2*, *vha-a3*, and *vha-a2 vha-a3* was measured as Concanamycin A-sensitive ATP hydrolysis. In both single mutants total V-ATPase activity was reduced and in the double mutant only the activity of TGN complexes containing VHA-a1 was detectable (Fig. 1*B*). In the same samples, V-PPase activity measured as KCl-stimulated PPi hydrolysis was found to be indistinguishable (Fig. 1*B*). Similarly, PPi-stimulated proton currents (Fig. 1*C*) recorded in the whole-vacuole configuration showed no significant difference in amplitude.

To determine how the lack of tonoplast V-ATPase affects vacuolar pH, we established an imaging approach using the ratiometric pH indicator 2′,7′-bis-(2-carboxyethyl)-5-(and-6)-carboxyfluorescein (BCECF) that was loaded into vacuoles of intact roots using its membrane-permeant acetoxymethyl (AM) ester. Confocal laser-scanning microscopy (CLSM) images of stained roots were analyzed (Fig. 1*D*) and the obtained ratios were converted to pH values using an in situ calibration curve (Fig. S5*A*). Whereas vacuoles in wild-type root cells had a pH of 5.9, *vha-a2 vha-a3* vacuoles were found shifted to pH 6.4 (Fig. 1*E*). Interestingly, morphology and size of vacuoles in *vha-a2 vha-a3* is indistinguishable from wild type, indicating that tonoplast V-ATPase activity is not required for vacuole biogenesis.

To corroborate these results with an independent method and to obtain information about vacuolar pH in different tissues, cell sap was extracted from rosette leaves of plants grown under long-day conditions (Fig. S5*B*). Whereas cell sap for wild type and the *vha-a3* single mutant was pH 5.8, the double mutant had a pH of 6.3.

**V-ATPase Activity Is Limiting for Vacuolar Ion Storage.** The rosette diameter of the double mutant is reduced and shows a striking dependence on day length, indicating that the photoperiod is limiting growth of *vha-a2 vha-a3* (Fig. 2*A*). Soil-grown plants use nitrate as the main source of nitrogen and once taken up into the cell, nitrate is partitioned between a small active cytosolic metabolite pool and a large storage pool in the vacuole (2). Nitrate accumulation within the vacuole is primarily mediated by the $NO_3^-/H^+$ exchanger AtCLCa and is dependent on the pH gradient (4). We thus investigated if the lack of tonoplast V-ATPase leads to a shift in the relative size of the two nitrate pools. HPLC analysis of rosette leaf extracts of 3-week-old plants grown in soil under 16-h light/8-h dark (long day, LD) cycles

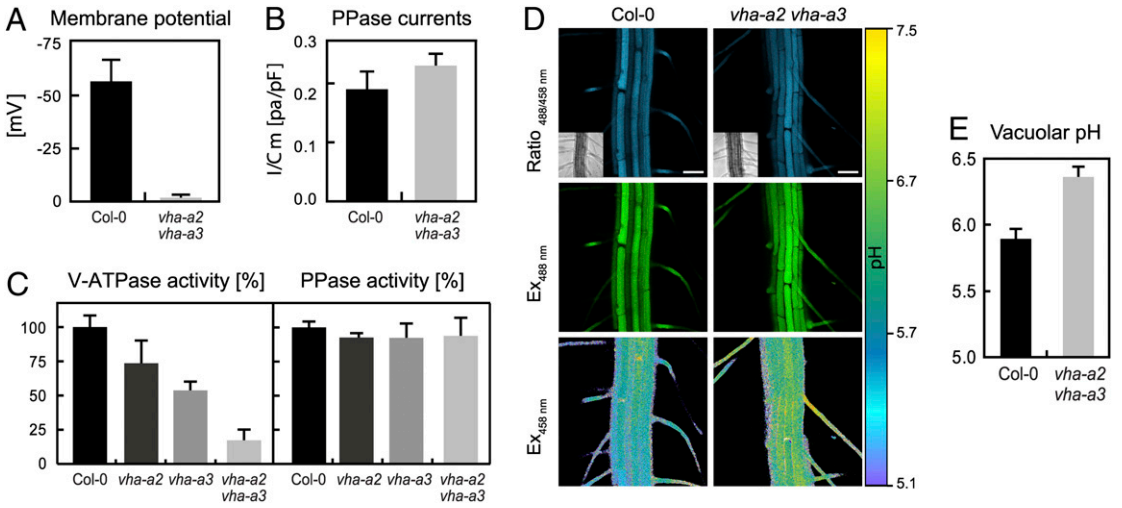


**Fig. 1.** Loss of tonoplast V-ATPase causes alkalinization of vacuolar pH. (*A*) ATP-induced membrane polarization of wild-type ($n = 5$) and *vha-a2 vha-a3* ($n = 3$) vacuoles. Error bars show SD. (*B*) $PP_i$-induced $H^+$ current densities from isolated vacuoles show similar values in wild type ($n = 3$) and *vha-a2-vha-a3* ($n = 5$). Error bars represent SD. (*C*) Concanamycin A-inhibited V-ATPase activity and $K^+$-stimulated PPase activity in microsomal membranes of 4-day-old etiolated seedlings. Wild-type activity was set to 100%. Error bars show SE of three independent experiments. (*D*) The images show emission intensities of epidermal root cell vacuoles loaded with BCECF AM. The ratio image of *vha-a2 vha-a3* indicates an increased vacuolar pH. (Scale bar, 50 μm.) (*E*) Loss of the tonoplast V-ATPase increases the vacuolar pH in root epidermal cells by 0.5 pH units. Error bars represent SE of 40 measurements from 20 seedlings.

revealed that *vha-a2 vha-a3* mutants contained ~80% less nitrate (Fig. 2*B*) and at the same time total nitrate reductase (NR) activity increased by ~90% (Fig. 2*C*). Accordingly, the double mutant contained more glutamine than wild-type plants (Fig. 2*D*).

Reduced leaf growth of the *vha-a2 vha-a3* double mutant under short- and long-day conditions is accompanied by varying degrees of leaf tip (Fig. 3*A*) and flower necrosis (Fig. S6), symptoms of calcium deficiency also found in the *cax1 cax3* mutant that lacks two vacuolar $Ca^{2+}/H^+$ antiporters (24, 25). In accordance, calcium content in leaf extracts of *vha-a2 vha-a3* plants grown in soil under LD conditions was >2-fold lower than in WT plants (Fig. 3*B*).

**Vacuolar Sequestration of Toxic Ions.** Proton-dependent transport at the tonoplast is important for nutrient storage but also for detoxification. The vacuolar membrane $Zn^{2+}/H^+$ antiporter MTP1 is important for zinc detoxification (26, 27) and we thus assayed zinc sensitivity of the *vha-a2 vha-a3* mutant (Fig. 3*C*). In the presence of 50 and 150 μM $ZnCl_2$, the mean root length of wild-type plants was reduced by 15 and 25%, respectively, whereas mutant roots showed a much stronger growth inhibition of 35 and 65% (Fig. 3*D*).

Plants deal with toxic sodium concentrations either by exclusion at the plasma membrane or by vacuolar sequestration mediated by $Na^+/H^+$ antiporters, presumably of the NHX family

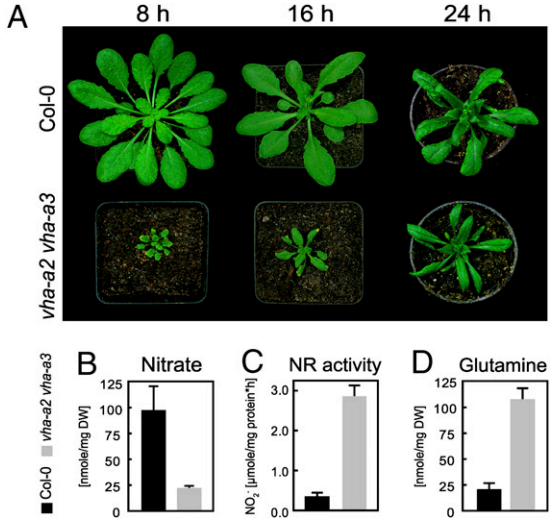


**Fig. 2.** Limited storage capacity for nitrate causes day-length-dependent growth reduction. (*A*) The *vha-a2 vha-a3* phenotype is severe if plants are grown under short-day conditions (8 h). Upon extended illumination periods (16 and 24 h) the growth phenotype is attenuated. Pictures show 7-week-old (8 h light) and 3-week-old (16 and 24 h light) plants. (*B*) Impaired vacuolar nitrate storage causes a reduction of the nitrate content in *vha-a2 vha-a3*. (*C*) Maximum nitrate reductase activity and (*D*) increased glutamine content in *vha-a2 vha-a3* are shown. (*B–D*) HPLC analysis and NR assay were performed on rosette leaves of 3-week-old plants grown in soil under 16-h light/8-h dark cycles. The plant material was collected 5 h after illumination started. Error bars represent SD of four biological replicates.

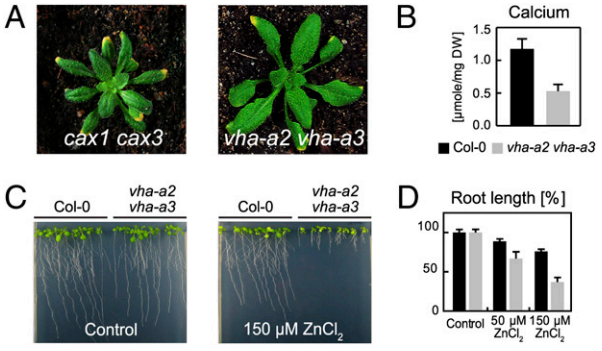


**Fig. 3.** Deficiency and toxicity symptoms in *vha-a2 vha-a3*. (*A* and *B*) *vha-a2 vha-a3* mutants display leaf tip necrosis and reduced calcium content similar to *cax1 cax3*. (*B*) HPLC analysis was performed on rosette leaves of 3-week-old plants grown in soil under a 16-h light/8-h dark cycle. Error bars represent SD of fouor biological replicates. (*C*) *vha-a2 vha-a3* mutants are hypersensitive against zinc. Seedlings were grown for 13 days under a 16-h light/8-h dark cycle on vertical plates containing different concentrations of $ZnCl_2$. (*D*) Root length. Error bar indicates SD of four replicate experiments. The control condition is set to 100%.

(6, 28). Accordingly, the reduced electrochemical proton gradient should render the *vha-a2 vha-a3* mutant more salt sensitive. However, we found that in the presence of increasing external concentrations of NaCl neither growth inhibition (Fig. 4*A* and Fig. S7*A*) nor accumulation of sodium, potassium, and chloride (Fig. 4 *B–D*) was significantly different from WT. To exclude that the unaffected salt sensitivity is due to compensation by increased activity of the V-PPase, we measured its activity and it appeared unchanged (Fig. 4*D*). Interestingly, the minor increase in V-PPase activity detected in WT plants grown under salt stress is not detected in the *vha-a2 vha-a3* mutant (Fig. 4*E*). The fact that reduced nitrate accumulation in the mutant is still observed under salt stress (Fig. 4*F*) also argues that the V-PPase is not able to compensate for a lack of V-ATPase activity.

**Endosomal V-ATPase and Salt Tolerance.** Many phenotypic aspects of the *det3* mutant are caused by reduced V-ATPase activity in the TGN/EE and not at the tonoplast (18). We thus next investigated if the increased salt sensitivity of *det3* (29) could be related to decreased acidification of the endosomal system. Indeed, root elongation of seedlings expressing an ethanol-inducible RNAi construct targeted against the TGN/EE-localized isoform VHA-a1 (18, 20) was inhibited in the presence of 25 mM NaCl (Fig. 4*G*), a concentration that does not significantly affect root growth in wild-type plants. At 50 mM NaCl (Fig. 4*H*), both transgenic lines analyzed showed increased growth inhibition correlating with the strength of the RNAi effect as observed previously (18).

## Discussion

Two vacuolar proton pumps, V-ATPase and V-PPase, energize the massive fluxes of ions and metabolites that are required for vacuolar functions throughout the plant life cycle. How the two pumps share the task of vacuolar acidification is a long-standing question in plant biology. The analysis of mutants lacking one of the two pumps has so far not contributed to solving this question because both enzymes have additional essential functions in endocytic and secretory trafficking. Here, we report on the characterization of an Arabidopsis mutant that lacks tonoplast V-ATPase activitv but has a functional V-ATPase in the TGN/EE. In contrast to loss-of-function alleles for ubiquitous V-ATPase subunits that cause either gametophytic or embryonic lethality (15, 16), the *vha-a2 vha-a3* mutant is viable. Thus V-ATPase activity in the TGN/EE is essential whereas V-ATPase-driven vacuolar acidification is at least not limiting during gametophyte and embryo development.

The phenotype of the *vha-a2 vha-a3* mutant thus uncovers the contribution of the V-PPase. When compared to wild type, vacuolar pH is increased by 0.5 units to 6.4. Assuming a cytosolic pH of 7.4, the proton concentration in mutant vacuoles is still 10-fold higher than in the cytosol. It remains to be determined if the remaining proton gradient is solely due to the activity of the V-PPase or if TGN/EE-derived vesicles acidified by the activity of VHA-a1 contribute to vacuolar acidification. As V-ATPase activity in the TGN/EE is required for endocytic and secretory trafficking, it will be challenging to differentiate between potential direct effects on vacuolar pH and indirect effects caused by reduced trafficking of proton pumps or other transporters. Lack of tonoplast V-ATPase activity does not lead to increased V-PPase activity. Interestingly, vacuolar pH in the *avp1* knock-out mutant was found to be increased by only 0.2–0.3 units (19), indicating that a lack of V-PPase activity might lead to increased V-ATPase activity.

Vacuolar nitrate storage and its subsequent remobilization are a central feature of a plant's nitrogen economy. Nitrate is stored in the vacuole during the night, when nitrate reductase is inactive. Our data suggest that reduced vacuolar uptake capacity can lead to increased cytosolic nitrate levels that in turn stimulate nitrate assimilation, a process that requires a substantial electron flow either via ferredoxin or NAD(P)H (30). The fact that reduced growth of the double mutant can be alleviated by increasing light periods thus likely reflects the metabolic burden imposed by continuous nitrate assimilation.

Salinity-induced increases in V-ATPase transcripts, protein levels, or activity have been reported in salt-tolerant as well as

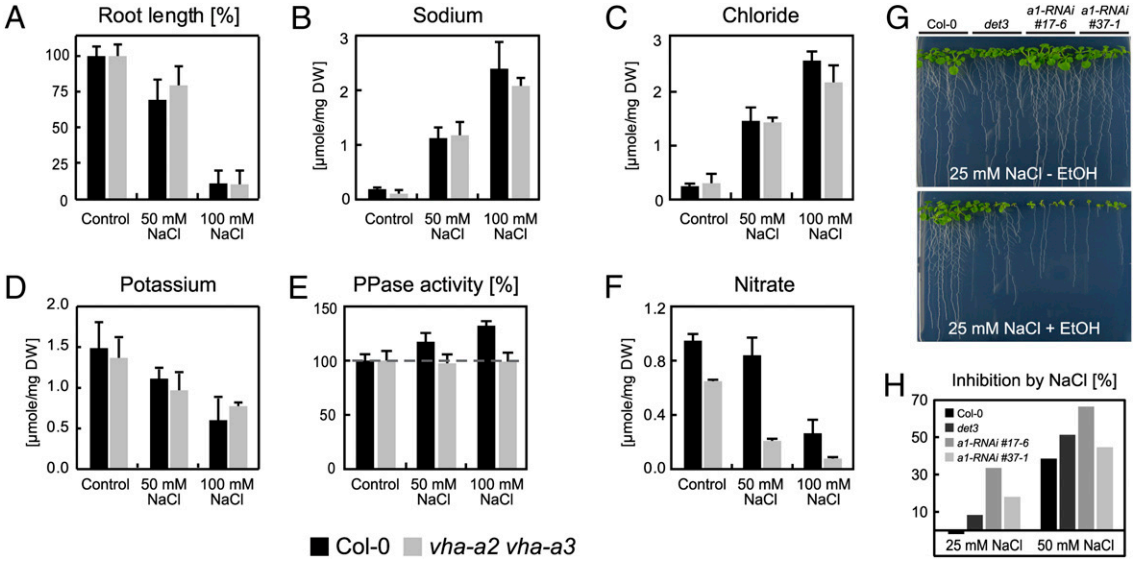


**Fig. 4.** The endosomal, but not the tonoplast V-ATPase is limiting under salt stress. (*A*) Inhibition of root growth through NaCl. The control condition was set to 100%. Error bars show SE with $n = 16$. Data are representative for one of three independent experiments. (*B–D* and *F*) HPLC analysis of sodium, chloride, potassium, and nitrate contents in 13-day-old seedlings grown on plates. Error bars represent SD of four biological replicates. (*E*) $K^+$-stimulated PPase activity was determined from microsomal membranes of 4-day-old etiolated Arabidopsis seedlings. Control activity was set to 100%. Error bars represent SE of three independent experiments. (*G*) A *RNAi* against *VHA-a1* was induced with 0.2% EtOH. Seedlings were grown for 15 days on vertical agar plates containing different concentrations of NaCl. The root length of the seedlings was measured (Fig. S7). (*H*) Inhibition of growth through salt upon EtOH induction. Differences between control samples (– EtOH) and treatment samples (+ EtOH) are expressed in percent.

salt-sensitive species including Arabidopsis, suggesting that increased V-ATPase level and/or activity may be required to drive $Na^+$ sequestration under salt stress (31). The finding that mutants with reduced V-ATPase activity have reduced salt tolerance supports this notion (29, 32). Moreover, subunits VHA-B1 and -B2 directly interact with salt-overly-sensitive (SOS)2, indicating that the Arabidopsis V-ATPase is a direct target of the SOS pathway (29). In the light of these results it is surprising that, at least under the conditions tested, tonoplast V-ATPase activity is not limiting for sodium accumulation. It has been reported that the cation selectivity ratio of AtNHX1 is regulated in a pH-dependent manner and it remains to be determined if the increased vacuolar pH in the *vha-a2 vha-a3* mutant favors $Na^+/H^+$ over $K^+/H^+$ exchange (33). However, potassium accumulation, relative to the wild type, was not reduced under salt stress in the double mutant, which argues against this explanation. It is becoming increasingly clear that the NHX family also includes endosomal transporters that play critical roles in $K^+$ homeostasis, luminal pH control, and vesicle trafficking (34). It will be of great interest to determine if the increased salt sensitivity of *VHA-a1* RNAi lines simply reflects that pH and ion homeostasis in the endosomal system is particularly sensitive to sodium or if endosomal $Na^+/H^+$ exchangers contribute to sodium detoxification. Indeed, the yeast $Na^+/H^+$ exchanger Nhx1p that contributes to sodium tolerance is localized in a late endosomal compartment (35, 36). In particular in meristematic cells that lack a central vacuole but also in fully differentiated cells an endosomal sodium-uptake system might be favorable because of its better surface-to-volume ratio.

We have shown here that although V-PPase activity is sufficient for embryo and seedling development, V-ATPase activity at the tonoplast is limiting for vegetative growth and reproductive development. Further analysis of vacuolar transport systems in the tonoplast V-ATPase-deficient background is required to provide important insight into the multifunctionality of plant vacuoles.

## Methods

**Plant Material and Growth Conditions.** *Arabidopsis thaliana* ecotype Col-0 seeds were grown in soil or on plates containing 1/10 Murashige–Skoog (MS) medium, 0.5% sucrose, and 10 mM Mes-KOH (pH 5.8) solidified with 1% phytoagar for vertical and 0.5% phyto agar for horizontal incubation. Plates prepared for mutants carrying an EtOH-inducible construct contained 0.2% EtOH. Phytoagar and MS basal salt mixture were purchased from Duchefa. Seeds were surface sterilized with EtOH or bleach and stratified for 48 h at 4 °C. Plants were grown at 22 °C with cycles of 16 h light and 8 h darkness unless indicated otherwise.

**Patch-Clamp Measurements on Isolated Mesophyll Vacuoles.** Fully developed rosette leaves of 5-week-old plants were used for daily protoplast isolation as described previously (37). Upon exposure to hypotonic medium [10 mM EGTA, 10 mM Hepes-Tris (pH 7.4) adjusted to 200 mosmol·$kg^{-1}$ with d-sorbitol] protoplasts burst and spontaneously released the vacuoles. The patch-clamp experiments were performed in the whole-vacuolar configuration basically as described in refs. 37 and 38. Current- and voltage-clamp measurements were carried out with an EPC-7 patch-clamp amplifier (HEKA) at a data acquisition rate of 1 ms and low-pass filtered at 0.2 or 1 kHz (8-pole low-pass bessel filter, Frequency Devices). Data were digitized by an ITC-16 interface (Instrutech), stored on a computer, and analyzed using the software programs Pulse and PulseFit (HEKA Elektronik) and IGORPro (Wave Metrics). Recordings were performed in agreement with the convention for electrical measurements on endomembranes (39). The whole-vacuolar currents were measured at the clamped voltage of 0 mV. To allow comparison of macroscopic current magnitudes among different vacuoles, the current densities ($I_{ss}/C_m$) were determined upon dividing the macroscopic ionic currents through the whole-vacuolar membrane capacitance $C_m$ of the individual vacuole. Bath and pipette solutions, which represent the cytosol and the vacuolar lumen for voltage-clamp recordings, were composed of 100 mM KCl, 5 mM $MgCl_2$, 1 mM $CaCl_2$, 2 mM DTT, and 10 mM Hepes-Tris (pH 7.5). The bath and pipette solutions for current-clamp recording contained 50 mM KCl, 5 mM $MgCl_2$, and 1 mM $CaCl_2$ and were adjusted to pH 6.5 and 7.5, respectively, by using either 10 mM Mes-Tris or 10 mM Hepes-Tris. Solutions were adjusted to an osmolality of 400 mosmol·$kg^{-1}$ with D-sorbitol. As indicated in the figure legends, the bath solution may additionally contain 5 mM Mg-ATP and/or 150 μM K-pyrophosphate (Sigma-Aldrich) freshly added from a stock solution.

**Protein Extraction.** For maximum NR activity measurements total proteins were extracted as described before (40). Plant material was pulverized in liquid nitrogen and extraction buffer (1 mL/g fresh weight [FW]) consisting of 0.25 M Tris-HCl (pH 8.0), 10 mM DTT, 10 μM FAD, 20 μM Leupeptin, and 10 mM $Na_2EDTA$ (pH 8.0). After thawing, the samples were briefly vortexed and centrifuged for 10 min at 4 °C with 18,000 × *g*. Microsomal membrane fractions were prepared as described in ref. 17 with minor modifications. Tissue was homogenized with 2.5 mL homogenization buffer per mg FW [350 mM sucrose, 70 mM Tris-HCl (pH 8.0), 10% (vol/vol) glycerol, 3 mM $Na_2EDTA$, 0.15% (wt/vol) BSA, 1.5% (wt/vol) PVP-40, 4 mM DTT, and 1× complete protease inhibitor mixture (Roche)]. The homogenate was filtered through two layers of Miracloth (Calbiochem) and centrifuged at 15,000 × *g* for 15 min at 4 °C. The supernatant was filtered through Miracloth again and then centrifuged at 100,000 × *g* for 1 h at 4 °C. The microsomal pellet was resuspended in 350 mM sucrose, 10 mM Tris-Mes (pH 7.0), 2 mM DTT, and 1× complete protease inhibitor mixture.

**Enzyme Activity Measurements.** V-ATPase and PPase activity of 10 μg microsomal membranes was colorimetrically determined as $P_i$ release (41) after an incubation period of 40 min at 28 °C. Reactions were terminated by adding 40 mM citric acid. For the blank value 10 μg BSA was used instead of microsomal protein. The V-ATPase assay medium contained 25 mM Tris-Mes (pH 7.0), 4 mM $MgSO_4 \times 7\ H_2O$, 50 mM KCl, 1 mM $NaN_3$, 0.1 mM $Na_2MoO_4$, 0.1% Brij 35, 500 μM $NaVO_4$, and 2 mM Mg-ATP. Activity was expressed as the difference between the measurements in the absence and the presence of 100 nM Concanamycin A. PPase activity was assayed in a reaction medium containing 25 mM Tris-Mes (pH 7.5), 2 mM $MgSO_4 \times 7\ H_2O$, 0.1 mM $Na_2MoO_4$, 0.1% Brij 58, and 0.2 mM $K_4P_2O_7$. PPase activity was calculated as the difference measured in the absence and the presence of 50 mM KCl.

Maximum nitrate reductase activity was determined after a modified protocol from ref. 40. The assay medium consisted of 0.05 M potassium phosphate buffer (pH 7.5), 10 mM $KNO_3$, 1 mM NADH-$Na_2$, and 10 mM $Na_2EDTA$ (pH 8.0). The reaction was started by adding 25 μL of the total protein in a volume of 250 μL assay buffer. To determine a blank value 25 μL of BSA (1 μg/μL) was used instead of the protein extract. After 20 min at 28 °C in darkness, the reaction was stopped by adding 50 μL of 1 M ZnAc. The samples were mixed vigorously and were incubated at room temperature (RT) for 20 min to oxidize excess NADH. Before nitrite detection samples were clarified by centrifugation. For the determination of nitrite a calibration curve with $KNO_2$ was prepared. The nitrite content of the samples was detected by adding 50 μL of 1% sulphanilamide (3 M HCl) and 50 μL of 0.02% *N*-(1-naphthyl)-ethylendiaminedihydrochloride to 50 μL of incubation mix. The ODs of the samples were read after 5 min at 540 nm in a microplate reader.

**pH Measurements.** Vacuolar pH of 5-day-old plate-grown seedlings was determined using the fluorescent cell-permeant dye BCECF AM (Molecular Probes). Loading of the dye was performed in liquid media containing 1/10 MS medium, 0.5% sucrose, and 10 mM Mes-KOH (pH 5.8) in the presence of 10 μM BCECF AM and 0.02% Pluronic F-127 (Molecular Probes). After 1 h of staining at 22 °C in darkness, the seedlings were washed once for 10 min in the media mentioned above. BCECF fluorescence was detected using a Zeiss Axiovert LSM510 Meta confocal laser-scanning microscope. The images were obtained using the LSM Confocal software and a Plan-Neofluar ×25 water immersion objective. The fluorophore was excited at 488 and 458 nm, respectively, and the emission was detected between 530 and 550 nm. All of the images were exclusively recorded within the root hair zone of fully elongated cells. Ratio images were generated using the ion concentration tool of the Zeiss LSM Confocal software and the images were processed using Adobe Photoshop software. The ratio values were obtained using the program ImageJ 1.41 (National Institutes of Health). The integrated pixel density was measured and the values of the 488-nm-excited images were divided by the values of the 458-nm-excited images. The ratio was then used to calculate the pH on the basis of a calibration curve (Fig. S5*A*).

**Metabolite Analysis.** Plant material was lyophilized and pulverized using a ball mill (Retsch). The powder was extracted with 80% methanol for 3 min at 99 °C and centrifuged at 20,000 × *g* for 3 min at room temperature. The supernatant was transferred in a new reaction tube and stored on ice. The residual pellet was extracted again with 20% methanol as described above. The supernatants were pooled and afterward completely dried in a vacuum

concentrator. For the analysis of amino acids the pellet was resuspended in lithium buffer (0.7% lithium acetate and 0.6% LiCl; Pickering Laboratories) with 0.2 mM norleucine as internal standard. The samples were clarified by centrifugation and filtered through a 0.22-μm Millex GV filter cartridge. Amino acids were separated by HPLC on a cation-exchange column with a flow rate of 0.34 mL/min (high-efficiency fluid column, 3 × 150 mm; Pickering Laboratories). Amino acids were derivatized with ninhydrine before photometric detection at 440 and 570 nm. For ion analysis the dried pellet was resuspended in water. The samples were clarified by centrifugation and filtered through a 0.22-μm Millex GV filter cartridge. A Dionex DX120 system equipped with suppressed conductivity detection was used in isocratic mode. For cation separation an Ion Pac-CS12A column (4 × 250 mm) was eluted with 20 mM methanesulfonic acid at a flow rate of 1 mL/min. Anions were separated on an Ion Pac AS 9-HC column (4 × 250 mm) with 9 mM sodium carbonate as mobile phase at a flow rate of 1 mL/min.

**ACKNOWLEDGMENTS.** We thank Bettina Stadelhofer and Mark Stahl (Center for Plant Molecular Biology, Universität Tübingen) for their expert help with the metabolite analysis as well as Zhao-Xing Wang, Elke Sauberzweig, Dagmar Ripper, and Beate Schöfer for technical assistance. This work was supported by the Deutsche Forschungsgemeinschaft through Grants FOR964+1061 (to K.S. and R.H.) and by King Saud University project money (to R.H. and K.A.S.A.-R.).

1. Martinoia E, Maeshima M, Neuhaus HE (2007) Vacuolar transporters and their essential role in plant metabolism. *J Exp Bot* 58:83–102.
2. Miller AJ, Fan X, Orsel M, Smith SJ, Wells DM (2007) Nitrate transport and signalling. *J Exp Bot* 58:2297–2306.
3. Schumaker KS, Sze H (1987) Decrease of pH gradients in tonoplast vesicles by NO(3) and Cl: Evidence for H-coupled anion transport. *Plant Physiol* 83:490–496.
4. De Angeli A, et al. (2006) The nitrate/proton antiporter AtCLCa mediates nitrate accumulation in plant vacuoles. *Nature* 442:939–942.
5. Blumwald E, Poole RJ (1985) Na/H antiport in isolated tonoplast vesicles from storage tissue of Beta vulgaris. *Plant Physiol* 78:163–167.
6. Apse MP, Aharon GS, Snedden WA, Blumwald E (1999) Salt tolerance conferred by overexpression of a vacuolar Na+/H+ antiport in Arabidopsis. *Science* 285:1256–1258.
7. Apse MP, Sottosanto JB, Blumwald E (2003) Vacuolar cation/H+ exchange, ion homeostasis, and leaf development are altered in a T-DNA insertional mutant of AtNHX1, the Arabidopsis vacuolar Na+/H+ antiporter. *Plant J* 36:229–239.
8. Hedrich R, Kurkdjian A, Guern J, Flugge UI (1989) Comparative studies on the electrical properties of the H+ translocating ATPase and pyrophosphatase of the vacuolar-lysosomal compartment. *EMBO J* 8:2835–2841.
9. Gaxiola RA, Palmgren MG, Schumacher K (2007) Plant proton pumps. *FEBS Lett* 581: 2204–2214.
10. Cipriano DJ, et al. (2008) Structure and regulation of the vacuolar ATPases. *Biochim Biophys Acta* 1777:599–604.
11. Maeshima M (2000) Vacuolar H(+)-pyrophosphatase. *Biochim Biophys Acta* 1465: 37–51.
12. Jaquinod M, et al. (2007) A proteomics dissection of Arabidopsis thaliana vacuoles isolated from cell culture. *Mol Cell Proteomics* 6:394–412.
13. Carter C, et al. (2004) The vegetative vacuole proteome of Arabidopsis thaliana reveals predicted and unexpected proteins. *Plant Cell* 16:3285–3303.
14. Nakanishi Y, Maeshima M (1998) Molecular cloning of vacuolar H(+)-pyrophosphatase and its developmental expression in growing hypocotyl of mung bean. *Plant Physiol* 116:589–597.
15. Dettmer J, et al. (2005) Essential role of the V-ATPase in male gametophyte development. *Plant J* 41:117–124.
16. Strompen G, et al. (2005) Arabidopsis vacuolar H-ATPase subunit E isoform 1 is required for Golgi organization and vacuole function in embryogenesis. *Plant J* 41: 125–132.
17. Schumacher K, et al. (1999) The Arabidopsis det3 mutant reveals a central role for the vacuolar H(+)-ATPase in plant growth and development. *Genes Dev* 13:3259–3270.
18. Brux A, et al. (2008) Reduced V-ATPase activity in the trans-Golgi network causes oxylipin-dependent hypocotyl growth inhibition in Arabidopsis. *Plant Cell* 20: 1088–1100.
19. Li J, et al. (2005) Arabidopsis H+-PPase AVP1 regulates auxin-mediated organ development. *Science* 310:121–125.
20. Dettmer J, Hong-Hermesdorf A, Stierhof YD, Schumacher K (2006) Vacuolar H+-ATPase activity is required for endocytic and secretory trafficking in Arabidopsis. *Plant Cell* 18: 715–730.
21. Alonso JM, et al. (2003) Genome-wide insertional mutagenesis of Arabidopsis thaliana. *Science* 301:653–657.
22. Borevitz JO, Xia Y, Blount J, Dixon RA, Lamb C (2000) Activation tagging identifies a conserved MYB regulator of phenylpropanoid biosynthesis. *Plant Cell* 12:2383–2394.
23. Daxinger L, et al. (2008) Unexpected silencing effects from T-DNA tags in Arabidopsis. *Trends Plant Sci* 13:4–6.
24. Cheng NH, Pittman JK, Barkla BJ, Shigaki T, Hirschi KD (2003) The Arabidopsis cax1 mutant exhibits impaired ion homeostasis, development, and hormonal responses and reveals interplay among vacuolar transporters. *Plant Cell* 15:347–364.
25. Cheng NH, et al. (2005) Functional association of Arabidopsis CAX1 and CAX3 is required for normal growth and ion homeostasis. *Plant Physiol* 138:2048–2060.
26. Desbrosses-Fonrouge AG, et al. (2005) Arabidopsis thaliana MTP1 is a Zn transporter in the vacuolar membrane which mediates Zn detoxification and drives leaf Zn accumulation. *FEBS Lett* 579:4165–4174.
27. Kobae Y, et al. (2004) Zinc transporter of Arabidopsis thaliana AtMTP1 is localized to vacuolar membranes and implicated in zinc homeostasis. *Plant Cell Physiol* 45: 1749–1758.
28. Qiu QS, et al. (2004) Regulation of vacuolar Na+/H+ exchange in Arabidopsis thaliana by the salt-overly-sensitive (SOS) pathway. *J Biol Chem* 279:207–215.
29. Batelli G, et al. (2007) SOS2 promotes salt tolerance in part by interacting with the vacuolar H+-ATPase and upregulating its transport activity. *Mol Cell Biol* 27: 7781–7790.
30. Lillo C (2008) Signalling cascades integrating light-enhanced nitrate metabolism. *Biochem J* 415:11–19.
31. Kluge C, et al. (2003) New insight into the structure and regulation of the plant vacuolar H+-ATPase. *J Bioenerg Biomembr* 35:377–388.
32. Padmanaban S, Lin X, Perera I, Kawamura Y, Sze H (2004) Differential expression of vacuolar H+-ATPase subunit c genes in tissues active in membrane trafficking and their roles in plant growth as revealed by RNAi. *Plant Physiol* 134:1514–1526.
33. Yamaguchi T, Aharon GS, Sottosanto JB, Blumwald E (2005) Vacuolar Na+/H+ antiporter cation selectivity is regulated by calmodulin from within the vacuole in a Ca2+- and pH-dependent manner. *Proc Natl Acad Sci USA* 102:16107–16112.
34. Pardo JM, Cubero B, Leidi EO, Quintero FJ (2006) Alkali cation exchangers: Roles in cellular homeostasis and stress tolerance. *J Exp Bot* 57:1181–1199.
35. Nass R, Cunningham KW, Rao R (1997) Intracellular sequestration of sodium by a novel Na+/H+ exchanger in yeast is enhanced by mutations in the plasma membrane H+-ATPase. Insights into mechanisms of sodium tolerance. *J Biol Chem* 272: 26145–26152.
36. Nass R, Rao R (1998) Novel localization of a Na+/H+ exchanger in a late endosomal compartment of yeast. Implications for vacuole biogenesis. *J Biol Chem* 273: 21054–21060.
37. Beyhl D, et al. (2009) The fou2 mutation in the major vacuolar cation channel TPC1 confers tolerance to inhibitory luminal calcium. *Plant J* 58:715–723.
38. Ivashikina N, Hedrich R (2005) K+ currents through SV-type vacuolar channels are sensitive to elevated luminal sodium levels. *Plant J* 41:606–614.
39. Bertl A, et al. (1992) Electrical measurements on endomembranes. *Science* 258: 873–874.
40. Fan X, Gordon-Weeks R, Shen Q, Miller AJ (2006) Glutamine transport and feedback regulation of nitrate reductase activity in barley roots leads to changes in cytosolic nitrate pools. *J Exp Bot* 57:1333–1340.
41. Heinonen JK, Lahti RJ (1981) A new and convenient colorimetric determination of inorganic orthophosphate and its application to the assay of inorganic pyrophosphatase. *Anal Biochem* 113:313–317.